

Run Group B Jeopardy Update Document

A. Avakian,³¹ L. Baashen,⁷ C. Dilks,³¹ F. Hauenstein,³¹ T. Hayward,³ A. Hobart,¹⁶ I. Ilieva,²⁹ J. Gilfoyle,²⁶
V. Kubarovsky,³¹ T. Kutz,²⁰ B. McKinnon,³⁵ S. Niccolai,^{16,*} S. Stepanyan,³¹ R. Tyson,³¹ and Z. Zhao⁴

¹Argonne National Laboratory, Argonne, Illinois 60439

²IRFU, CEA, Université Paris-Saclay, F-91191 Gif-sur-Yvette, France

³University of Connecticut, Storrs, Connecticut 06269

⁴Duke University, Durham, North Carolina 27708-0305

⁵Fairfield University, Fairfield CT 06824

⁶Università di Ferrara, 44121 Ferrara, Italy

⁷Florida International University, Miami, Florida 33199

⁸The George Washington University, Washington, DC 20052

⁹Idaho State University, Pocatello, Idaho 83209

¹⁰INFN, Sezione di Ferrara, 44100 Ferrara, Italy

¹¹INFN, Laboratori Nazionali di Frascati, 00044 Frascati, Italy

¹²INFN, Sezione di Genova, 16146 Genova, Italy

¹³INFN, Sezione di Roma Tor Vergata, 00133 Rome, Italy

¹⁴INFN, Sezione di Torino, 10125 Torino, Italy

¹⁵INFN, Sezione di Pavia, 27100 Pavia, Italy

¹⁶IJCLAB, CNRS/IN2P3, Université Paris-Saclay, 91405 Orsay, France

¹⁷Institute für Kernphysik (Juelich), Juelich, Germany

¹⁸Kyungpook National University, Daegu 41566, Republic of Korea

¹⁹Lamar University, 4400 MLK Blvd, PO Box 10009, Beaumont, Texas 77710

²⁰Massachusetts Institute of Technology, Cambridge, Massachusetts 02139-4307

²¹Mississippi State University, Mississippi State, MS 39762-5167

²²National Research Centre Kurchatov Institute - ITEP, Moscow, 117259, Russia

²³Norfolk State University, Norfolk, Virginia 23504

²⁴Ohio University, Athens, Ohio 45701

²⁵Old Dominion University, Norfolk, Virginia 23529

²⁶University of Richmond, Richmond, Virginia 23173

²⁷Università di Roma Tor Vergata, 00133 Rome Italy

²⁸Skobeltsyn Institute of Nuclear Physics, Lomonosov Moscow State University, 119234 Moscow, Russia

²⁹University of South Carolina, Columbia, South Carolina 29208

³⁰Temple University, Philadelphia, PA 19122

³¹Thomas Jefferson National Accelerator Facility, Newport News, Virginia 23606

³²Universidad Técnica Federico Santa María, Casilla 110-V Valparaíso, Chile

³³Università degli Studi dell'Insubria, 22100 Como, Italy

³⁴Università degli Studi di Brescia, 25123 Brescia, Italy

³⁵University of Glasgow, Glasgow G12 8QQ, United Kingdom

³⁶University of York, York YO10 5DD, United Kingdom

³⁷University of Virginia, Charlottesville, Virginia 22901

³⁸College of William and Mary, Williamsburg, Virginia 23187-8795

³⁹Yerevan Physics Institute, 375036 Yerevan, Armenia

(Dated: April 9, 2024)

I. INTRODUCTION

The CLAS12 Run Group B comprises eight experiments, 4 approved and rated by the PAC and 4 run-group proposals, sharing the same target type (liquid deuterium) and beam (11 GeV polarized electrons). They are listed in Table I.

The physics objectives of Run-Group B are manifold:

- 3D nucleon structure studies (FFs, PDFs, TMDs, GPDs) using deuterium as a neutron target and measuring exclusive and semi-inclusive reactions. Main goals: access to the GPD E, leading to the contribution of quarks' angular momentum to the nucleon spin; flavor separation of GPDs and TMDs via combination of proton and deuteron observables; accurate measurement of the neutron magnetic form factor at high Q².

* Contact person: silvia@jlab.org

Experiment number	Title	Contact person	PAC days (rating)
E12-07-104	Neutron magnetic form factor	G. Gilfoyle	30 (A-)
E12-09-007a	Study of parton distributions in K SIDIS	W. Armstrong	56 (A-)
E12-09-008	Boer-Mulders asymmetry in K SIDIS	M. Contalbrigo	56 (A-)
E12-11-003	Deeply virtual Compton scattering on the neutron	S. Niccolai	90 (A High Impact)
E12-09-008b	Collinear nucleon structure at twist-3 in dihadron SIDIS	M. Mirazita	RG
E12-11-003a	In medium structure functions, SRC, and the EMC effect	O. Hen	RG
E12-11-003b	Study of J/ψ photoproduction off the deuteron	Y. Ilieva	RG
E12-11-003c	Quasi-real photoproduction on deuterium	F. Hauenstein	RG

TABLE I. The eight experiments of Run Group B.

- Exclusive, near-threshold coherent and incoherent J/Ψ quasi-real photoproduction on deuteron, to study the gluonic structure of bound nucleons and the deuteron, and search for isospin partners of the LHCb pentaquark.
- In-medium structure functions, Short Range Correlations, and the EMC effect, studied via proton-DIS with neutron-spectator tagging, to be compared to free-proton DIS results.
- Quasi-real $p\bar{p}$ photoproduction to look for $p\bar{p}$ resonances and study the coherent production mechanism on deuterium

The beam time allocated for Run-Group B is 90 PAC days, corresponding to the time assigned to the nDVCS experiment. The nDVCS experiment was labeled as High Impact by PAC 41, with the motivation that "once the scaling for Deep Exclusive Scattering is established, the highest goal of the GPD program is understanding of the nucleon's angular momentum carried by quarks, through the measurement of the nucleon helicity-flip GPD (E)." (PAC41 report). Run-Group B has so far obtained 39 out of the 90 awarded PAC days. In order to optimize the science impact of JLab, allocating the remaining time is essential to reach the necessary accuracy to extract E on a vast phase space.

II. EXPERIMENTAL SETUP

Run-group B uses the CLAS12 spectrometer in its baseline configuration, plus the Forward Tagger (FT), the RICH, and the Central Neutron Detector (CND), which were all already installed and commissioned before the first CLAS12 experiment (RG-A). In addition, the Backward Angles Neutron Detector (BAND) was installed right before the beginning of the experiment. The CLAS12 cryogenic target (5-cm long), filled with liquid deuterium (D2) at 23 K, is used.

III. OVERVIEW OF THE THREE RUN PERIODS

RG-B has run during three periods of roughly one calendar month each, between the end of winter 2019 and the beginning of 2020, for a total of about 38.9 PAC days. The average beam polarization was about 85%, with variations of a couple of percent during the different run periods.

A. Spring 2019

The experiment ran from February 8 to March 25 2019. The first half had a beam energy of 10.6 GeV, which was subsequently lowered to 10.2 GeV, from March 8 onwards, due to accelerator problems. From the beam-time accounting of CEBAF:

- Available Beam in Use (ABU): 522.8 hours
- Beam Available but Not Used (BANU): 79.1 hours
- Beam Not Available (BNA): 374.6 hours.

Thus, this run achieved a total of 21.7 PAC days according to ABU. Roughly 9.7 B triggers at 10.6 GeV and 11.7 B at 10.2 GeV were collected, with the CLAS12 torus in inbending configuration.

B. Fall 2019

The experiment ran from December 3 to December 20 2019. The beam energy was, this time, 10.4 GeV. From the beam-time accounting of CEBAF:

- ABU: 161.6 hours
- BANU: 36 hours
- BNA: 184.8 hours.

This run corresponded to 6.7 PAC days according to ABU. Roughly 9.0 B triggers were collected, with the CLAS12 torus in outbending configuration.

C. Winter 2020

The experiment ran from January 7 to January 29 2019. The beam energy was 10.4 GeV. From the beam-time accounting of CEBAF:

- ABU: 244.7 hours
- BANU: 35.2 hours
- BNA: 281.3 hours.

This run corresponded to 10.5 PAC days according to ABU. Roughly 12.9 B triggers were collected, with the CLAS12 torus in inbending configuration.

IV. RESULTS

A. Ratio Measurement of the Neutron Magnetic Form Factor G_m^n

The elastic electromagnetic form factors are basic observables that describe the distribution of charge and magnetization inside the proton and neutron. Their measurement is a goal of the 2015 NSAC Long-Range Plan and it forms a central part of the physics program at JLab. We are part of a broad campaign to measure the four elastic, electromagnetic, nucleon form factors (electric and magnetic ones each for the proton and neutron) at JLab that includes seven experiments approved for running during the 12 GeV era.

We use the ratio R of $e-n$ to $e-p$ events in quasi-elastic (QE) kinematics to extract G_M^n . This ratio method is less sensitive to experimental parameters like luminosity, electron reconstruction efficiency, trigger efficiency, *etc.* We then use the precisely known proton magnetic and electric form factors (G_M^p and G_E^p) along with the small contribution of the neutron electric form factor (G_E^n) to determine G_M^n from the equation for R . We apply acceptance matching to insure both event types have the same acceptance. We use the measured electron information and, assuming QE kinematics, calculate both proton and neutron trajectories through CLAS12. If both calculated trajectories strike the detector fiducial volume we keep the event. Preliminary results for R for one beam energy (there are runs at three different beam energies) are shown in the left-hand panel of Fig. 1. The measured results (red) vary smoothly up to $Q^2 = 12 \text{ GeV}^2$. The blue points are the same points with their statistical uncertainties scaled by the factor we expect for full running of the remaining Run Group B beam time. With a bit more than twice as many events the uncertainties are significantly reduced. The added statistics may also add another point at high Q^2 .

There are corrections required before we extract G_M^n . The most important is the neutron detection efficiency (NDE) to correct the $e-n$ yield. It is one of the largest components of the G_M^n systematic uncertainty. Comparison of past measurements at different laboratories reveals considerable tension among those experiments possibly due to variations in detector performance and efficiency. To measure the NDE we use the $^1\text{H}(e, e'\pi^+n)$ reaction on a hydrogen target from Run Group A data in CLAS12. This reaction is a source of tagged neutrons which can be detected in the electromagnetic calorimeter of CLAS12. We start with the $^1\text{H}(e, e'\pi^+X_n)$ reaction where X_n can be multiple neutral particles. These neutrals are neutron candidates. We use the measured electron and pion kinematics to predict the candidate neutron path through CLAS12. This track is the expected neutron. We then search the event for neutral hits near the intersection point of the expected track with the front face of the CLAS12 calorimeters and select the hit closest to the predicted trajectory.

We fit the missing mass distributions as a function of neutron momentum p_n to extract the neutron yield. The NDE is the ratio of detected to expected neutrons as a function of neutron momentum. The right-hand panel in Fig. 1 shows some of our results. The NDE rises steeply at low p_n and in the neutron momentum region relevant to the G_M^n analysis our fits with different functions converge to a plateau with $\text{NDE} \approx 0.79$. This consistency implies our systematic uncertainties are under control.

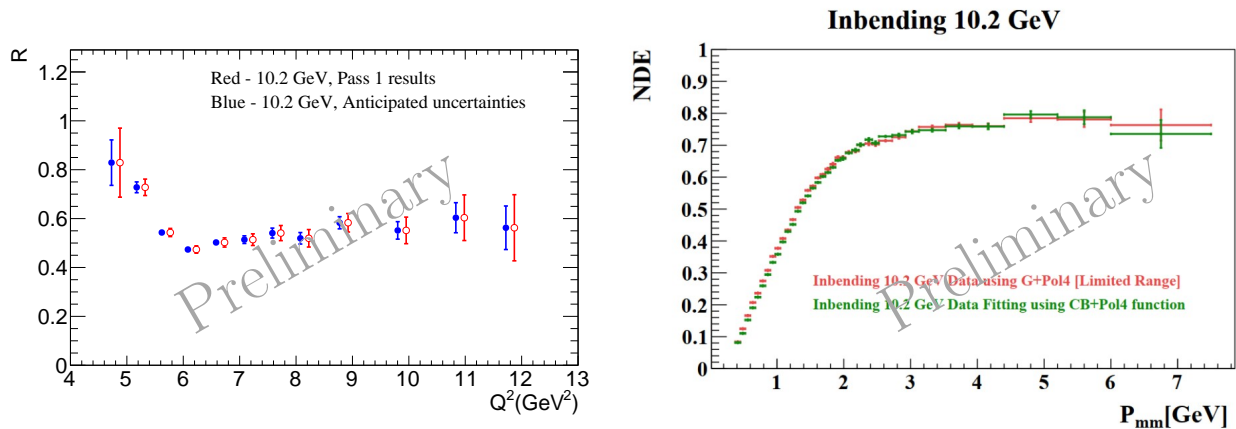


FIG. 1. The ratio R of $e-n/e-p$ events (left-hand panel) is shown for one electron beam energy with the measured statistical uncertainties (red) and the anticipated ones for full running (blue). The Q^2 for the blue points is shifted slightly to make both points visible. The neutron detection efficiency (NDE) is shown (right-hand panel) for the same beam energy for two choices of the function used to fit the neutron missing mass peak.

The analysis is far along. Since 2020 a group consisting of G.P.Gilfoyle (University of Richmond), B.A.Raue, and L.A.Baashen (Florida International University) has been extracting G_M^n from CLAS12 data. The analysis is Dr. Baashen's thesis experiment and she defended it in November, 2023. Several corrections to the ratio R remain and the group continues to work toward publication.

B. nDVCS

Measuring Deeply Virtual Compton Scattering on a neutron target is one of the necessary steps to complete our understanding of the structure of the nucleon in terms of Generalized Parton Distributions (GPDs). DVCS on a neutron target allows to operate a flavor decomposition of the GPDs and plays a complementary role to DVCS on a transversely polarized proton target in the determination of the GPD E , the least known and least constrained GPD that enters Ji's angular momentum sum rule [1].

The importance of neutron targets in the DVCS phenomenology was clearly established in the pioneering Hall A experiment, where the polarized-beam cross section difference off a neutron, from a deuterium target, was measured [2]. This experiment was recently followed by a second, higher-statistics, analysis of 6-GeV Hall A [3] data on deuterium target. This analysis leads to a model-dependent extraction of three combinations of Compton Form Factors (CFFs, which are integrals of GPDs) separated into quark flavors, via a measurement of the nDVCS cross section at two different beam energies. One of the limits of both Hall-A nDVCS experiments is the lack of exclusivity: only the electron and the photon are detected, and the $e\gamma$ yield is obtained by subtracting proton target data from deuteron target data, and removing the background from coherent deuteron DVCS with a missing-mass selection cut. While the semi-inclusive detection topology ($e\gamma X$) allows to achieve a high statistical accuracy, sizeable systematic uncertainties remain due to the subtraction procedures. Moreover, the kinematics reach of the Hall-A experiments was limited by the low electron-beam energy.

This experiment aims to perform, for the first time, a fully exclusive extraction of the neutron-DVCS reaction by detecting the recoiling neutron. It will measure, over a wide phase space, the beam-spin asymmetry (BSA), which has a direct sensitivity to E , the least known and constrained GPD. Furthermore, the high energy electrons of the upgraded CEBAF permits to cover unexplored kinematics, in particular the low- x_B region, where models, such as VGG [4], predict the BSA to be sizeable, and high Q^2 , where the leading-twist GPD formalism can be applied.

The full analysis of data taken during RG-B period has been performed, the results were approved by the Collaboration and will be submitted to PRL. Although the available statistics allowed only for one-dimensional binning in

the phase space, the results for nDVCS are very promising and provided a clear separation in terms of flavour of the GPD E; with more data, a multidimensional scan of BSA in the phase space will become possible.

Several cuts were applied in order to ensure proper particle identification and select the relevant kinematic region for the DVCS reactions. Exclusivity cuts were applied to select the $e'n\gamma(p)$ final state while minimizing the background coming from partially reconstructed π^0 decays from $ed \rightarrow e'n\gamma\pi^0(p)$, where only one of the two photons from the π^0 decay is reconstructed. Figure IV B shows examples of exclusivity variables for the data (in blue) and the simulations (in red). It is important to note that in spite of the exclusivity cuts, the data still contain some background originating from the partially reconstructed π^0 decay.

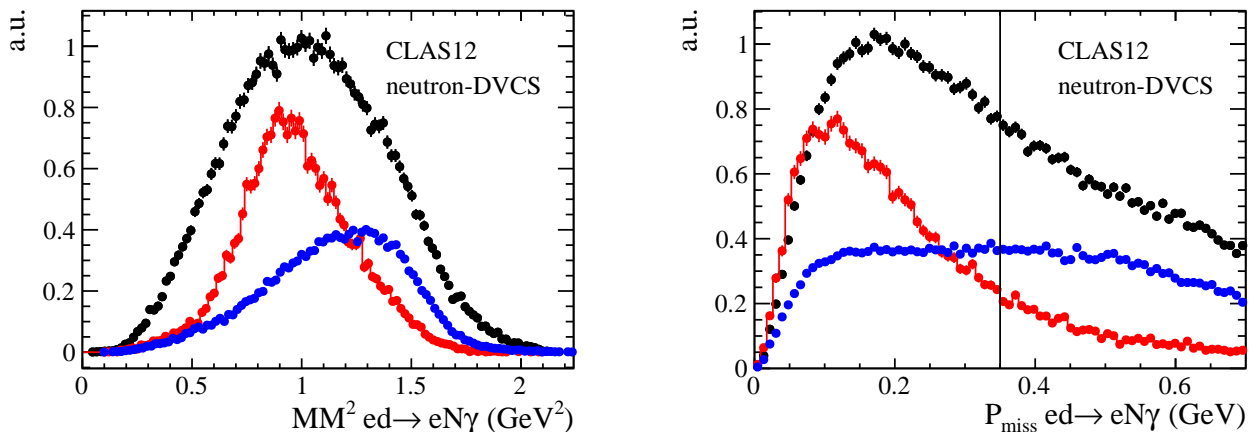


FIG. 2. Left: squared missing mass from $ed \rightarrow e'n\gamma X$. Right: missing momentum from $ed \rightarrow e'n\gamma X$, the line defines the chosen cut. The data (black) are compared with simulations of neutron DVCS (red) and of partially reconstructed π^0 background (blue).

Due to local inefficiencies in the Central Tracker, some protons were misidentified as neutrons. This background was reduced using a multivariate analysis technique (Boosted Decision Trees) which relied on low-level features from the CND and the CTOF as well as on one final-state exclusivity variables. The leftover contamination from protons to the neutron sample was estimated to be $\sim 5\%$ and subtracted in the computation of the BSA.

Figure 3 shows the kinematic coverage in Q^2 and x_B after applying all selection cuts. The BSA, which was extracted in bins of either Q^2 , x_B or t , is plotted as a function of ϕ in Fig. 4. The systematic uncertainties, represented by the red histogram, are consistently smaller than the statistical ones. The BSA has the expected sinusoidal shape arising from the DVCS-BH interference. Its amplitude is of the order of a few percent, about a factor of 4 smaller than the proton-DVCS $\sin \phi$ amplitude measured at these same kinematics. Figure 5 shows the amplitude (A_{LU}) of the $\sin \phi$ fits to the BSA, as a function of Q^2 (left), x_b (middle) and $-t$ (right). The x_B distribution is compared to

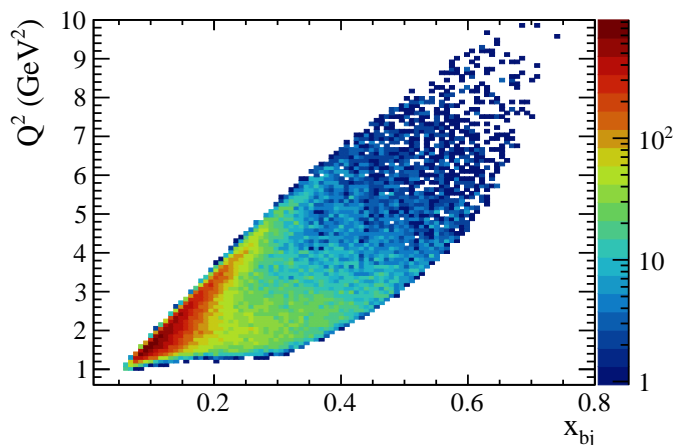


FIG. 3. Q^2 versus x_B for the nDVCS data sample with all selection cuts applied, showing the wide kinematic reach of CLAS12.

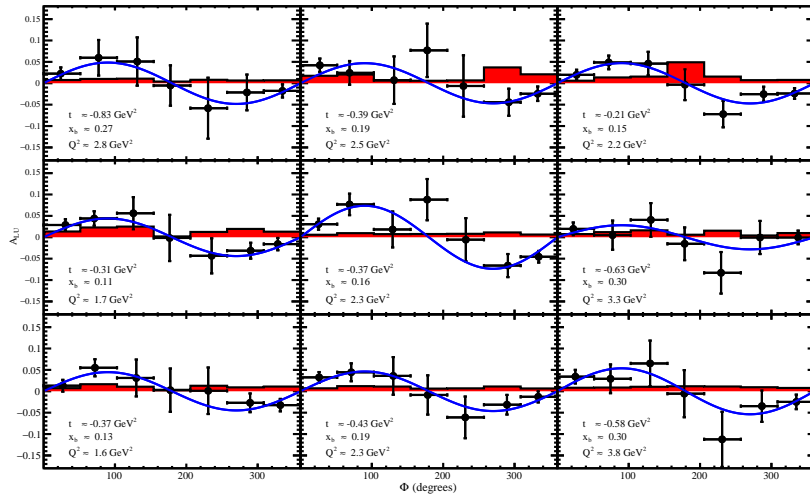


FIG. 4. Beam-spin asymmetry from nDVCS versus ϕ , for (bottom) three bins in Q^2 ($[1, 1.9]$, $[1.9, 2.9]$, and $[2.9, 6]$ GeV^2), (middle) three bins in x_B ($[0.05, 0.14]$, $[0.14, 0.2]$, and $[0.2, 0.6]$), and (top) three bins in $-t$ ($[0, 0.3]$, $[0.3, 0.5]$, and $[0.5, 1.1]$ GeV^2). The data are fit with the function $(a \sin(\Phi))$ (blue line). The red histogram shows the total systematic uncertainty.

predictions of the VGG model [4] for different values of the quarks' total angular momenta J_u and J_d . In the VGG framework, the CLAS12 data rule out negative values of J_d , which the model predicts to yield negative asymmetries. The $J_u = 0.2$, $J_d = 0$ hypothesis (pink dotted line in Fig. 5) is also excluded by the data. The size of the statistical error bars does not allow to distinguish between the two other cases examined ($J_u = 0.3$ $J_d = 0.1$, solid green line, and $J_u = 0.1$ $J_d = 0.1$, dashed blue line).

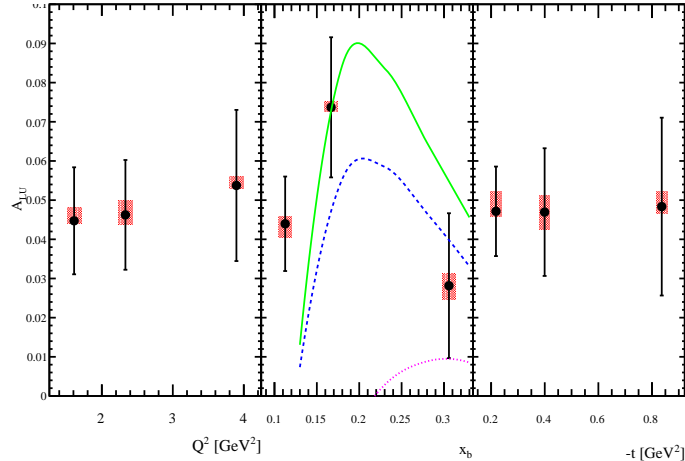


FIG. 5. $\sin \phi$ amplitude of the beam-spin asymmetry for neutron DVCS as a function of Q^2 (left), x_B (middle) and $-t$ (right). The red bands represent the systematic uncertainties. The VGG model predictions for different values of J_u and J_d are compared to the BSA versus x_B : solid green line for $J_u = 0.3$ $J_d = 0.1$, dashed blue line for $J_u = 0.1$ $J_d = 0.1$, and pink dotted line for $J_u = 0.2$ $J_d = 0$.

The sensitivity of the CLAS12 nDVCS BSA to GPDs, in particular to the imaginary part of E was tested by including the measured observable in a non-biased fit method, based on neural nets, to extract CFFs [?]. In this method CFFs are parametrized as neural networks, with values at input representing the kinematical variables x_B and t , and values at output representing the imaginary or real parts of CFFs. Figure 6 shows the extracted up and down quark $\Im m \mathcal{H}$ and $\Im m \mathcal{E}$ CFFs, extracted by fit to old CLAS and HERMES proton data, to recent CLAS12 proton data and to the neutron DVCS data reported here. The flavored models used for Fig. 6 have 200 trained neural nets to optimize the statistics. Note that the Hall A neutron DVCS data were not included in this study. While the CLAS12 nDVCS data show some unexpected impact on flavor separation of $\Im m \mathcal{H}$, the main new result is a clean flavor separation of $\Im m \mathcal{E}$. The same CFF extraction method was previously used to attempt flavor separation

of the CFFs of H and E by combining pDVCS data and the Hall A nDVCS results [?]. While promising results were obtained for $\Re\mathcal{H}$ and $\Im\mathcal{H}$, the separation was not possible for E . The small systematics uncertainties of the CLAS12 nDVCS data, obtained mainly thanks to the detection of the active neutron, and their wide kinematic coverage provide the necessary sensitivity to the flavor separation of $\Im\mathcal{E}$.

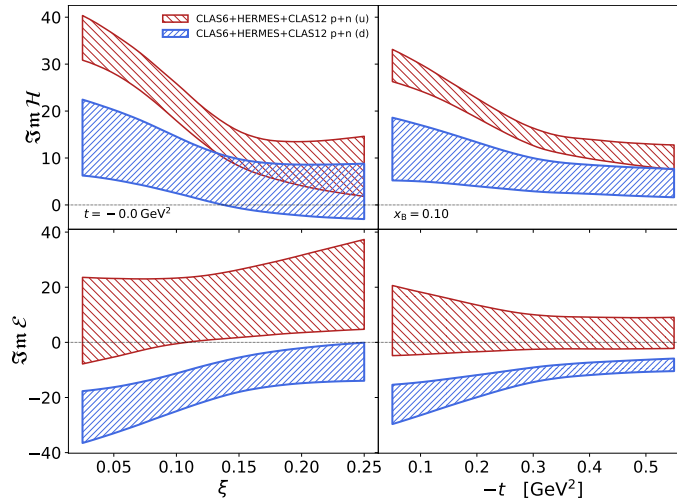


FIG. 6. Extraction of up (u , red) and down (d , blue) quark contributions to $\Im m \mathcal{H}$ (top) and $\Im m \mathcal{E}$ (bottom), as a function of ξ (left) and $-t$ (right).

The result shown are obtained combining runs taken with 10.6, 10.4 and 10.2 GeV beam energy. Combining BSAs obtained with different beam energies is a complex operation, due to the strong beam-energy dependence of the Bethe-Heitler cross section. Depending on the kinematics, and especially at the edges of the ϕ distribution, the nDVCS/BH cross section can vary strongly following a variation of 400 MeV in the beam energy. Although the BSA is less sensitive than the cross section to the beam energy (as the BSA is proportional to the DVCS/BH interference term), the steep variation of the cross section affects the value of the central kinematics for each bin, making the combination of the three datasets, therefore, includes model-dependent systematic uncertainties. It will be crucial to have a stable, high-statistics run, possibly at one of the beam energies already used, for the remainder of the data taking.

C. Semi-inclusive deep inelastic scattering

1. *dSIDIS (back-to-back) dihadron production*

The vast majority of semi-inclusive deep inelastic scattering (SIDIS) research has predominantly concentrated on the study of hadron production in the current-fragmentation region (CFR), where hadrons in the final state originate from the impacted quark. According to Quantum Chromodynamics (QCD), the generation of hadrons within the CFR is delineated through a factorized scheme, involving the convolution of parton distribution functions (PDFs) with fragmentation functions (FFs) [5]. In this context, PDFs elucidate the likelihood of encountering a particular quark or gluon in a specific state within the nucleon [6, 7], while FFs detail the process of hadron formation from quarks and gluons. Nonetheless, hadrons emerging in the target-fragmentation region (TFR), which are produced with the involvement of spectator partons, do not fit into this framework and have remained largely unexplored. The theoretical groundwork for analyzing the TFR leverages the fracture function formalism, initially established for the collinear scenario in Ref. [8]. This methodology has since been extended to encompass spin- and transverse-momentum-dependent scenarios [9]. Fracture functions are utilized to describe the conditional probability of forming a specific hadron in the final state from the target remnant following the ejection of a certain quark. Pioneering measurements from RGA (liquid hydrogen target) have recently published a first observation of a signal sensitive to TMD fracture functions [10] in Physical Review Letters. This measurement reported on the observation of spin-dependent azimuthal asymmetries in back-to-back dihadron electroproduction in deep inelastic scattering.

The first-time observation of a non-zero A_{LU} in back-to-back SIDIS suggests that long-range spin-orbit correlations between CFR and TFR hadrons could be substantial. Our method of measuring correlations between the target and current-fragmentation regions introduces a novel approach to quantifying the interplay between the spin and transverse

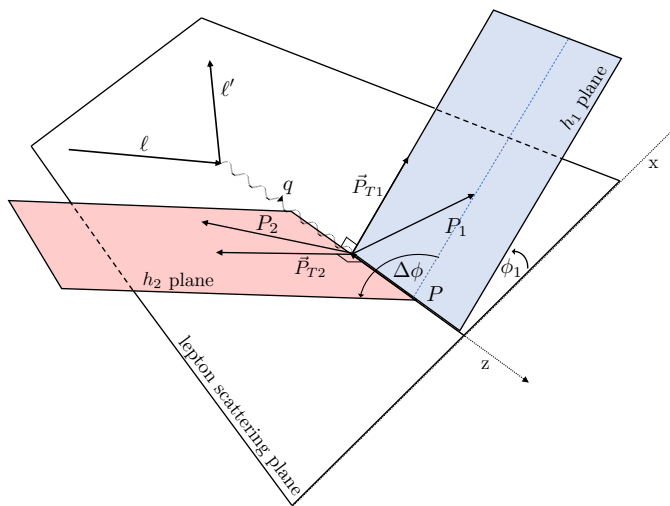


FIG. 7. The SIDIS kinematics of back-to-back dihadron production in the center-of-mass frame. The x - z plane is defined by the incoming and outgoing lepton with positive z in the direction of the virtual photon. ϕ_1 and ϕ_2 are defined from the scattering plane to P_1 and P_2 in an anti-clockwise direction.

momenta of quarks within the nucleon, opening new pathways for exploring the intricate nucleonic structure through quark and gluon interactions. The kinematics of these observed asymmetries fall outside the perturbative regime; they are more likely to stem from the entanglement between the longitudinally polarized struck quark and the target remnant [9].

Following the pioneering efforts to publish the initial observation of a TMD FrF dependent observable, considerable work has been undertaken to prepare a sequel publication intended for Physical Review D (PRD). This analysis, now in an advanced phase, aims to explore the flavor dependence within the back-to-back channel. It will likely mark the first utilization of “pass-2” data. The upcoming study is set to include nearly triple the amount of $ep \rightarrow e'p\pi^+X$ data collected using a liquid hydrogen target. Moreover, it will extend its investigation to the negative pion channel, $ep \rightarrow e'p\pi^-X$, and delve into target flavor dependence through the analysis of deuterium in the reactions $ed \rightarrow e'p\pi^+X$ and $ed \rightarrow e'p\pi^-X$. This combination of hydrogen and deuterium data, only possible by leveraging measurements from both run groups, enables the possibility of studying the flavor dependence of the fracture functions.

On the left side of Fig. 8, the preliminary integrated back-to-back asymmetry is depicted for each of the four channels. A marginal difference is noted between the two targets, which can be ascribed to the back-to-back asymmetry and the associated fracture functions predominantly reflecting a valence quark effect that is dominated by u-quark contributions. The outcome is significantly influenced by whether the virtual photon interacts with a u- or d-quark, determining the nature of the resulting hadrons. Conversely, the magnitude of the asymmetry in negative pion channels is approximately half of that observed in the positive pion scenario. This disparity can be rationalized by examining the pion production mechanisms via fragmentation functions. Whereas π^+ pions are generally produced either directly or through decay of vector mesons like the ρ , which originate from struck u-quarks, π^- pions receive competing contributions from directly produced hadrons from struck d-quarks or decays of these same ρ -mesons generated from u-quarks. This competition diminishes the overall magnitude relative to the positive pion channel.

A further facet of this follow-up analysis is the access to significantly enhanced statistics. This increased statistics will facilitate multidimensional studies previously unfeasible in the initial publication. The dependence on Q^2 is of specific interest. It is predicted that the back-to-back $\sin\Delta\phi$ asymmetry should manifest as a twist-2 object, and the observed Q^2 dependence of the asymmetry, illustrated on the right side of Fig. 8, corroborates this prediction. The strong correlations between Q^2 and other variables, in particular x_B , necessitates as high statistics as possible in order to study the Q^2 dependence.

2. Current Fragmentation Dihadron Production

In dihadron SIDIS production, two hadrons are detected in the final state in the current fragmentation region together with the scattered electron. The additional degree of freedom present in the two-hadron final state allows for the study of many additional quantities not available in a single hadron analysis (or in the dSIDIS case where both hadrons have separate kinematic origins). The SIDIS dihadron electroproduction cross section expansion depends

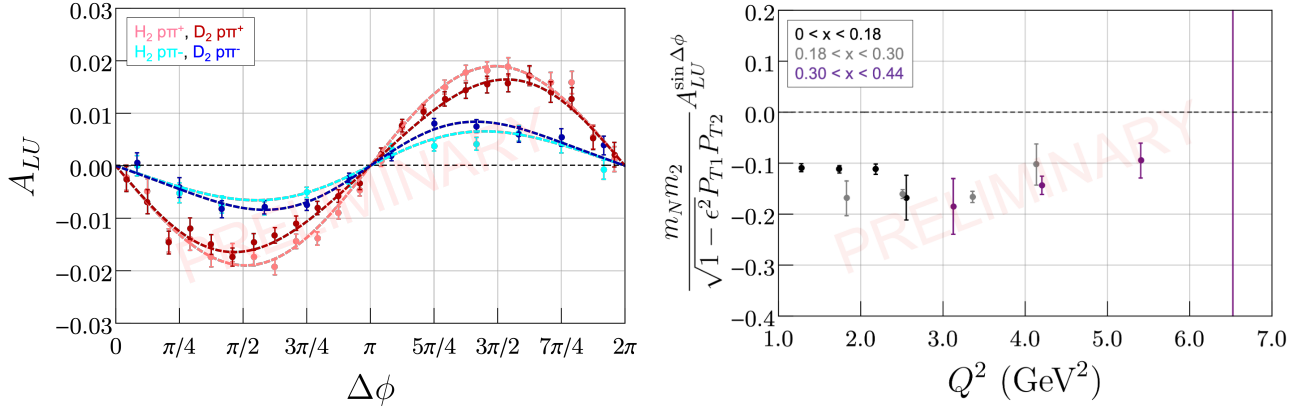


FIG. 8. Left: the preliminary integrated back-to-back asymmetries for the $ep \rightarrow e'p\pi^+X$ (light red), $ed \rightarrow e'p\pi^+X$ (dark red), $ep \rightarrow e'p\pi^-X$ (light blue) and $ed \rightarrow e'p\pi^-X$ (dark blue) as a function of $\Delta\phi$. Right: the preliminary $ep \rightarrow e'p\pi^+X$ back-to-back asymmetry as a function of Q^2 in bins of x .

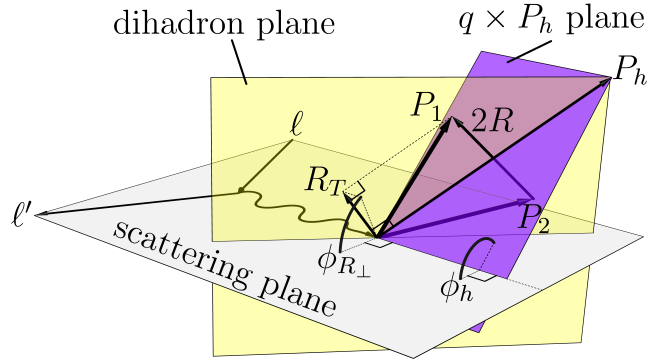


FIG. 9. The coordinate system used in this analysis. The electron scattering plane is spanned by the incoming and outgoing lepton, the dihadron plane is spanned by P_1 and P_2 , containing also P_h , R , and R_T , and the $q \times P_h$ plane contains only q and P_h . The azimuthal angles ϕ_h and $\phi_{R\perp}$ are defined within the plane transverse to q , from the electron scattering plane to, respectively, the $q \times P_h$ plane and the dihadron plane.

on structure functions that are associated with sinusoidal modulations in ϕ_h and $\phi_{R\perp}$, pictured in Figure 9. Data taken in the fall of 2018 with the CLAS12 spectrometer using a 10.6 GeV longitudinally spin-polarized electron beam delivered by CEBAF at JLab resulted in the first ever CLAS12 publication [11]. Our work involved the simultaneous extraction of seven different azimuthal modulations, described in Table II, each of which contains a structure function with a convolution of a TMD and a DiFF [12]. The DiFFs can be further expanded into partial waves on the basis of spherical harmonics [12] which results in modulations of $\cos\theta$ (where θ can loosely be thought of as the dihadron decay angle).

One way to gain understanding of the interaction between quarks and gluons in the nucleon is to study the subleading twist PDFs. One such quantity is the collinear twist-3 PDF $e(x)$ [13, 14]. As a subleading PDF, $e(x)$ does not possess a straightforward probabilistic interpretation but its moments provide significant insight: the first x -moment of $e(x)$ represents the contribution to the nucleon mass from the finite quark masses [13, 15, 16], and the third x -moment is proportional to the transverse force experienced by a transversely polarized quark in an unpolarized nucleon immediately after scattering [17, 18]. Previous model-dependent extractions of $e(x)$ from single-hadron data have been performed [19] along with preliminary extractions from two-pion data from CLAS [15, 20]. In SIDIS single-hadron production, $e(x)$ is only accessible via beam spin asymmetries with the inclusion of the transverse momentum dependence (TMD) of the FF which leads to a convolution of the PDF and FF over the TMD. Additionally, factorization of the cross section into PDFs and FFs in the TMD framework is not yet proven at subleading twist [21]. These issues motivated the high-precision measurement of these two-pion beam spin asymmetries.

As this was only a first observation, significant extensions of this analysis are not only possible but already in the works. A follow up, long-form paper is currently in progress to extend the results of the $ep \rightarrow e'p\pi^+\pi^-$ analysis to a

twist	m	partial waves	modulation	PDF \otimes FF
2	0	0, 0, 1, 0, 2, 0	0	0
2	± 1	1, ± 1 , 2, ± 1	$\sin(\phi_h - \phi_{R\perp})$	$f_1 \otimes G_{1,OT}^\perp, f_1 \otimes G_{1,LT}^\perp$
	± 2	2, ± 2	$\sin(2\phi_h - 2\phi_{R\perp})$	$f_1 \otimes G_{1,TT}^\perp$
3	0	0, 0, 1, 0, 2, 0	$\sin(\phi_h)$	$e \otimes H_{1,OO}^{\perp ss+pp}, e \otimes H_{1,OL}^\perp, e \otimes H_{1,LL}^\perp$
	1	1, 1, 2, 1	$\sin(\phi_{R\perp})$	$e \otimes H_{1,OT}^\triangleleft, e \otimes H_{1,LT}^\triangleleft$
3	-1	1, -1, 2, -1	$\sin(2\phi_h - \phi_{R\perp})$	$e \otimes H_{1,OT}^\perp, e \otimes H_{1,LT}^\perp$
	2	2, 2	$\sin(-\phi_h + 2\phi_{R\perp})$	$e \otimes H_{1,TT}^\triangleleft$
	-2	2, -2	$\sin(3\phi_h - 2\phi_{R\perp})$	$e \otimes H_{1,TT}^\perp$

TABLE II. Table of A_{LU} modulations, organized by twist and m . For each value of m , the available partial waves are listed, along with, respectively, the PDF and FF convolutions to which the A_{LU} modulation amplitudes are sensitive. Note that at twist 2, the $m = 0$ modulation is zero, and the amplitude for any $m > 0$ is equal to that of $-m$. At subleading twist the \triangleleft and \perp notations correspond to positive and negative values of m .

full partial wave decomposition [22]. The dihadron production cross-section can be further expanded into partial waves on the basis of spherical harmonics, where instead of integrating over θ (the dihadron decay angle), the associated Legendre polynomials, $P_{\ell,m}(\cos\theta)$, are included in the asymmetry fits. This breaks the ambiguity present in Table II where individual quantum numbers, m , can correspond to the combination of multiple convolutions of PDFs and FFs. This additional information, combined with the now significantly increased statistics (approximately 4x as much or more) will enable a rich multidimensional extraction of dipion partial waves. Several preliminary results on this expansion have already been shown in conference proceedings [23]. In particular, preliminary results for the leading twist single spin asymmetries as a function of the invariant pair mass are shown in FIG. 10. The $A_{LU}^{1,1}$ and $A_{LU}^{\perp,1}$ asymmetries shown in the left hand side of the plot correspond to the azimuthal modulations $\sin\theta \sin(\phi_h - \phi_{R\perp})$ and $\sin\theta \cos\theta \sin(\phi_h - \phi_{R\perp})$ which are the analog of the single $\sin(\phi_h - \phi_{R\perp})$ modulation when θ is not integrated over. The significantly increased statistics and more advanced fitting techniques allow for the exciting possibility to fully extract these quantities for the very first time.

Another further extension of this analysis involves comparing results on the proton target with data taken on deuterium. Correlators, such as PDFs like $e(x)$, can exhibit significant flavor dependence and so comparisons between SIDIS off the proton and neutron (accessible in deuterium target studies) are vital for a complete understanding of nucleonic structure. The PDF $e(x)$ is of particular interest, because model predictions about the relative contribution of the up and down quarks to the total distribution function differ substantially [24–26]. The $\sin\phi_{R\perp}$ modulation is proportional to [27]

$$A_{LU}^{\sin\theta \sin\phi_{R\perp}} \Big|_{\text{proton}} \propto \frac{(4xe^u(x) - xe^d(x)) H_1^{\triangleleft 1,1}}{(4f_1^u(x) + f_1^d(x)) D_1^u(z, M_h)} \quad (1)$$

$$A_{LU}^{\sin\theta \sin\phi_{R\perp}} \Big|_{\text{deuterium}} \propto \frac{3(xe^u(x) - xe^d(x)) H_1^{\triangleleft 1,1}}{5(f_1^u(x) + f_1^d(x)) D_1^u(z, M_h)}, \quad (2)$$

for the proton and deuterium target cases respectively. With the combination of the initial observation of two pion beam spin asymmetries [11] produced from a proton target and the ongoing measurement with deuterium targets a point-by-point extraction of the flavor decomposition of $e(x)$ becomes possible. Comparable statistics for CLAS12 data exists for deuterium targets as for the proton (which already includes a significant increase from the statistics used in the first CLAS12 publication) which will allow for a full multidimensional partial wave analysis and flavor decomposition. A preliminary result for this comparison is shown in FIG. 11 which indicates approximately equal asymmetry amplitudes between both targets. Although further work is still needed, this preliminary result favors models where the up and down contributions to $e(x)$ are not similar.

D. Tagged DIS measurements with BAND

Deep inelastic scattering measurements, tagged by the detection of a high-momentum spectator neutron, allows the study of the bound proton structure function F_2^{*p} when that proton is in a high-momentum, highly-virtual state. We will extract the ratio of the bound to free proton structure function as a function of spectator neutron light-cone momentum fraction α_s , by measuring ratios of high- x' to low- x' $d(e, e'n)X$ events (x' is the Bjorken scaling variable

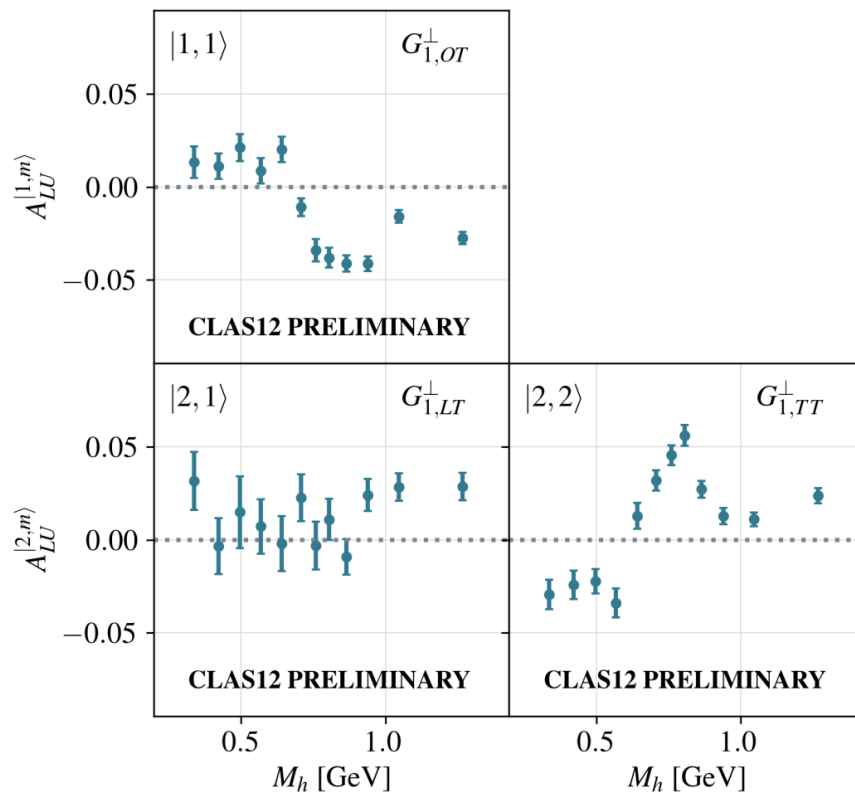


FIG. 10. Preliminary results of the leading twist single spin asymmetries in the dipion channel with a full partial wave expansion up to $\ell = 2$. The two left hand plots correspond to the single right hand plot of $A_{LU}^{\sin(\phi_h - \phi_{R^\perp})}$ in FIG. ?? but, here, with the inclusion of the information on the decay angle θ . This analysis breaks the ambiguity between the $G_{1,OT}$ and $G_{1,LT}$ partial waves of the helicity dependent dihadron fragmentation function.

for a moving nucleon). Comparing the ratio with theoretical predictions allows one to disentangle the various effects (nucleon motion, short-range correlations, binding) to the modification of the structure function.

The tagged DIS observable in our current analysis is proportional to a ratio of experimental yields,

$$R_{exp}(\alpha_S, x') = Y_{exp}(\alpha_S, x')/Y(\alpha_S, x' = 0.3) \quad (3)$$

where $Y_{exp}(\alpha_S, x')$ is simply the number of neutron-tagged $d(e, e'n)$ counts in a given (α_S, x') bin meeting all event selection, PID, fiducial, and DIS kinematic cuts.

From existing RGB data, we have extracted the experimental ratio in four α_S bins covering the range $1.15 < \alpha_S < 1.5$ (corresponding to spectator neutron momenta of approximately $150 < p_n < 450$ MeV/c). In each α_S bin, the ratio is extracted up to $x' = 0.65$ (bin center). The existing yields in these bins are shown in blue in Figure 12. The same figure also shows the projected yields for the full RG-B approved beamtime, in red. The increased statistics could either be used for finer (α_S, x') bins, or simply to decrease the statistical uncertainty in the existing bins.

Further, the additional beamtime could allow an extension of the tagged DIS analysis to even higher α_S . Figure 13 shows the current (blue) and projected (red) yields for an additional bin covering $1.5 < \alpha_S < 1.6$. With the full approved RG-B beamtime, the statistics in this bin would be comparable to the existing statistics in our current highest α_S bin ($1.5 < \alpha_S < 1.6$).

E. J/ψ Photoproduction off Deuteron

The objective of this scientific program is to measure the differential cross-section of (a) the incoherent, (b) the coherent production of J/ψ meson off the deuteron, and (c) the cross-section of J/ψ production off the neutron. The program aims to address several interesting physics aspects of the J/ψ production dynamics that cannot be answered by measurements off a proton target. The RGB experiment provides the very first measurement of exclusive

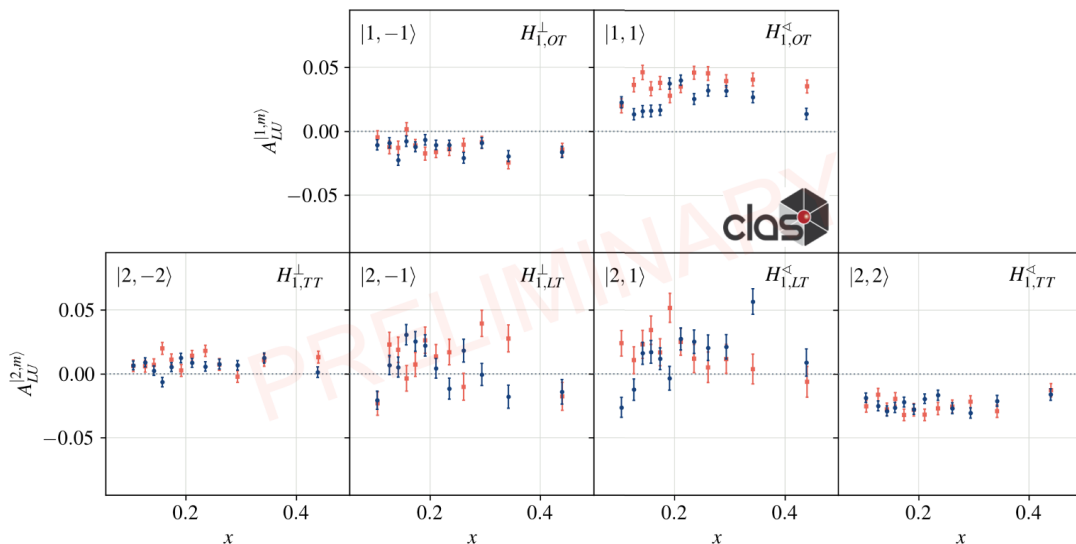
Twist-3 A_{LU} Amplitudes

FIG. 11. Preliminary comparisons between proton target (red) and deuterium target (blue) two pion single spin asymmetries at subleading twist with a full partial wave expansion up to $\ell = 2$. The $A_{LU}^{1,1}$ asymmetry is the analog of the left hand side of asymmetry used to extract $e(x)$. Comparisons between the two asymmetries will allow for a point by point extraction of the up and down quark contributions to $e(x)$.

J/ψ photoproduction off deuteron from threshold up to 11 GeV. By measuring the unexplored quasi-free (QF) J/ψ photoproduction off the neutron, we aim to test the isospin invariance of the J/ψ production mechanism near-threshold and explore other, non-gluonic exchange, production mechanisms. With sufficient statistics, the data will provide evidence for (or against) a pentaquark decaying into $J/\psi n$. We aim to assess the largely unknown low-energy total $J/\psi N$ cross-section using models (e.g., VMD) to access the $J/\psi N$ elastic scattering in final-state interactions directly. Last but not least, measuring coherent J/ψ production would provide a first glimpse into the nuclear gluon distribution a decade before the advent of the Electron-Ion Collider (EIC).

The J/ψ proposal joined RGB in 2018, and the relevance and significance of all three components of the proposed studies continue to be high. The nuclear aspect of the program remains unique as there are no other competing data or expected exclusive experiments on deuteron or light nuclear targets.

The recent publications by the GlueX [28, 29] and the J/ψ -007 [30] collaborations sparked a renewed interest in the near-threshold J/ψ production mechanism. Models assuming a dominant two-gluon exchange have been shown to adequately describe the near-threshold J/ψ cross section [31, 32]. These are of particular interest as they relate the J/ψ cross-section to the gluonic Gravitational Form Factors (gGFFs) of the nucleon [30, 33–35] that describe the internal shear force, pressure, and mass distributions of the gluonic content of the nucleon. However, features of the total and differential cross sections measured by GlueX seem to indicate non-negligible contributions from intermediate open-charm states such as $\Lambda_c \bar{D}^{(*)}$ [29, 36, 37]. Comparing J/ψ photoproduction off the proton and the neutron in RGB allows to test the isospin invariance of the J/ψ production mechanisms, with two-gluon exchange being isospin invariant but not necessarily contributions from open-charm intermediate states. If the contribution to the cross-section from the intermediate open-charm states dominates that of the two-gluon exchange at certain energy ranges, then the J/ψ production cross-section may be different on the neutron and proton. In the case of a dominant two-gluon exchange, a first measurement of J/ψ photoproduction on the neutron in RGB would allow us to estimate the gGFFs of the neutron.

The reactions $\gamma d \rightarrow J/\psi pn$ and $\gamma d \rightarrow J/\psi d$ are being measured in untagged quasi-real photoproduction, where all the final state particles (the nucleon(s) or deuteron, and the lepton pair from the J/ψ decay) are detected in the CLAS12 forward detector. Machine learning algorithms were developed to identify the decay leptons. The interacting beam photon and the undetected scattered electron kinematics are deduced from the 4-momentum conservation. The invariant mass of missing particles must be consistent with that of the undetected scattered electron. The scattered electron kinematics were restricted to very forward angles to ensure quasi-real photoproduction (consequently, the virtuality of the interacting photon $Q^2 \simeq 0$). J/ψ can then be identified in the di-lepton invariant mass. The

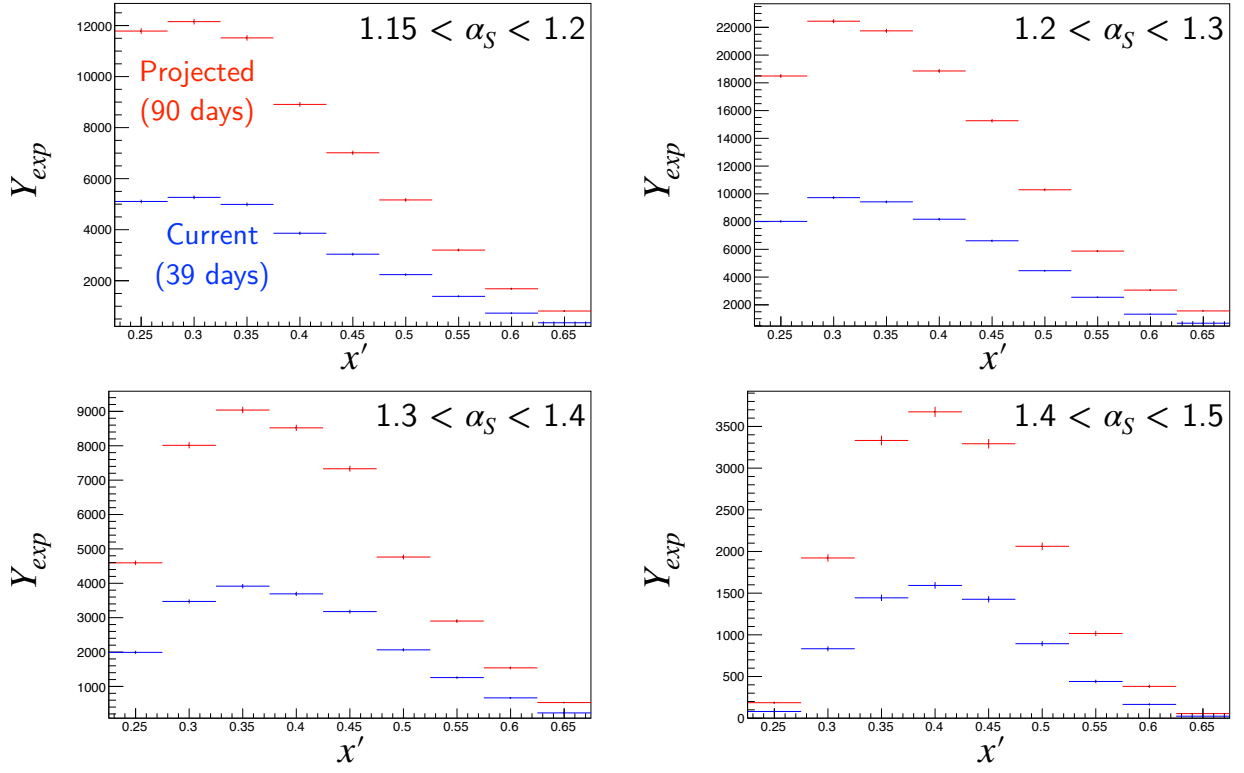


FIG. 12. Experimental $d(e, e'n)$ yields in the current tagged DIS analysis bins, from existing RG-B data (blue), and projected to the full RG-B approved beamtime (red).

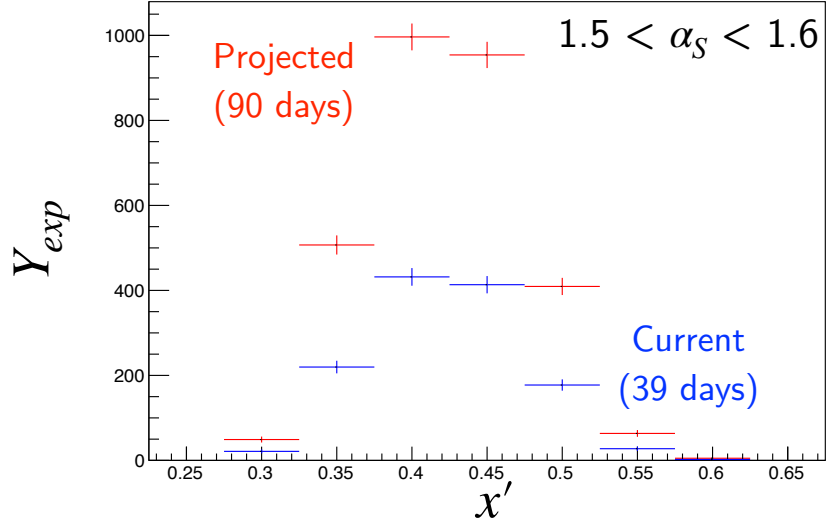


FIG. 13. Experimental $d(e, e'n)$ yields in a new α_S bin, from existing RG-B data (blue), and projected to the full RG-B approved beamtime (red).

comparison of J/ψ photoproduction on the proton and neutron has been prioritized to the measurement of J/ψ production on the deuteron since the latter has lower production rates and limited statistics. Shown in Figure 14 is the invariant mass of e^+e^- and $\mu^+\mu^-$ produced on the proton and neutron. More stringent requirements on particle identification are necessary to identify J/ψ produced on the neutron in its decay to $\mu^+\mu^-$, which in turn reduces the statistics available for analysis. For now, the comparison of the J/ψ cross-section on proton and neutron is limited to the decay channel to e^+e^- .

Figure 15 shows the total cross section measured in several bins of photon energy, E_γ . The cross-sections on

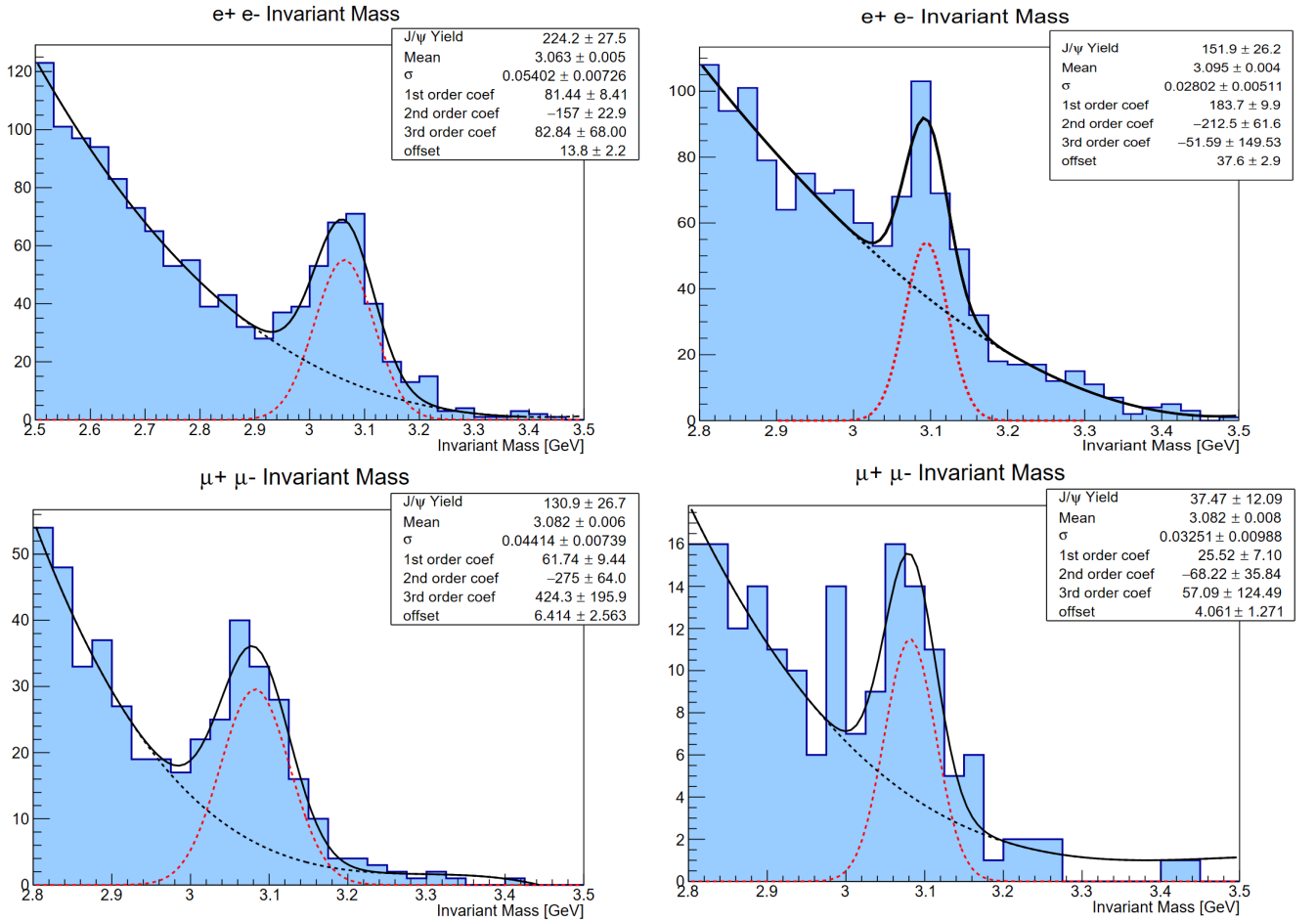


FIG. 14. The invariant mass of e^+e^- (top row) and $\mu^+\mu^-$ (bottom row), produced on the proton (left column) and neutron (right column). The invariant mass is fitted with a third-order polynomial and a Gaussian.

the proton and neutron are preliminary and shown in arbitrary units. The good agreement within the statistical uncertainty of the total cross-section on the proton and neutron suggests that whatever production mechanism is at play must be isospin invariant, or if isospin invariance is broken, the effect is smaller than the reported statistical uncertainty.

Figure 15 was produced using the spring 2019 dataset only, which corresponds to 21.7 PAC days, roughly a quarter of the total allocated beam time and slightly over half of the already collected beam time. Running the remaining beam time for RG-B is crucial in order to deliver statistically significant results for the three physics topics of interest. The structures in the GlueX cross-section that suggest contributions to the cross-section from intermediate open-charm states are visible in the energy range from 8.7 GeV to 9.5 GeV. Improved statistical accuracy for the J/ψ production cross-section determination is imperative for studies of the neutron gGFF and assessing the contribution of intermediate open charm states to J/ψ near-threshold photoproduction.

F. New analyses: pDVCS in deuterium

In addition to the original proposals, the RG-B data have been analyzed for new first-time measurements.

In particular, an analysis has been performed to extract incoherent proton DVCS on a deuterium target. The interest for this channel is twofold:

- to understand nuclear-medium effects on GPDs, along the line of the experiments being carried out at CLAS on He^4 [38]
- a comparison between free-proton pDVCS and incoherent pDVCS on deuterium will help extract the free-neutron nDVCS from the incoherent one.

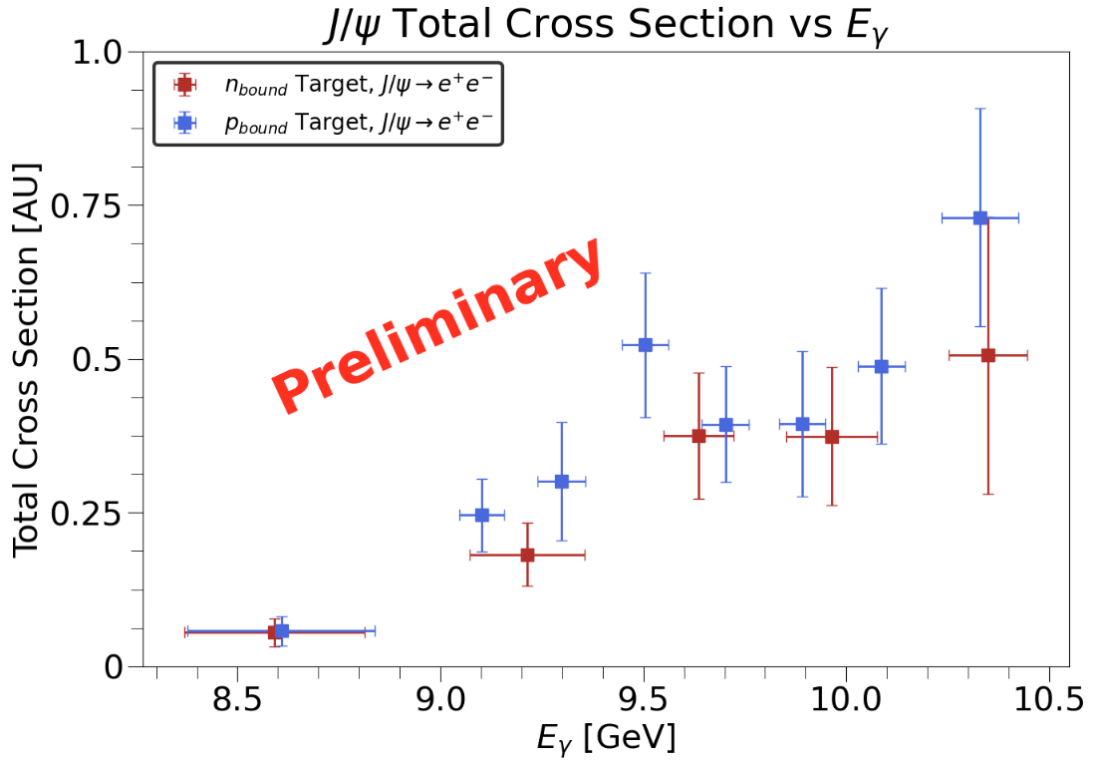


FIG. 15. The total J/ψ photoproduction cross section produced on the proton (blue) and neutron (red) with J/ψ decaying to e^+e^- . The results are preliminary and shown in arbitrary units.

The analysis with Pass1 data has been completed and approved by the analysis review committee (see Fig.16). The work should go for publication after performing a thorough comparison with the free proton DVCS. As for nDVCS, data from different periods with different beam energies have been combined together. For the remainder of the beam team, it is crucial to have a high-statistics run at one of the beam energies already used with preference to 10.6 GeV as the one used during the free-proton DVCS experiment.

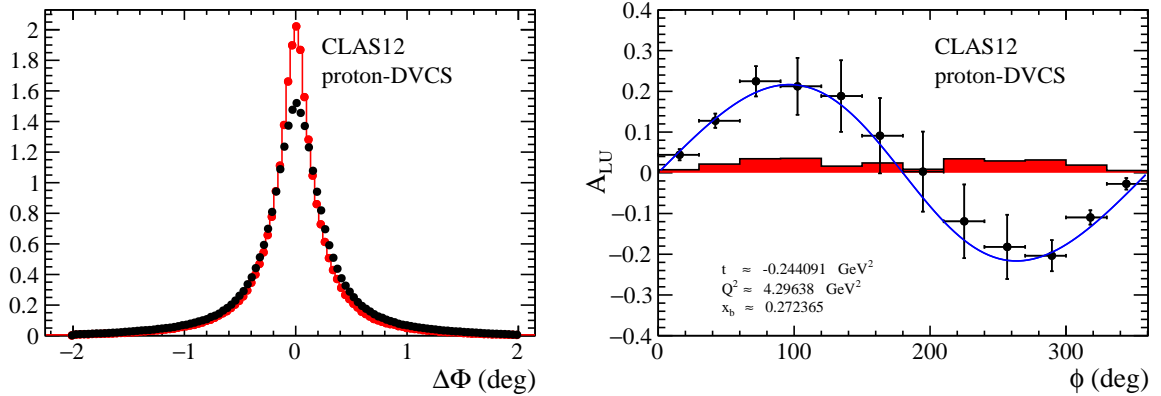


FIG. 16. Left: the difference between two ways of calculating the Trento angle Φ compared between signal (black) and simulation (red). Right: BSA for the incoherent proton DVCS on a deuterium target in a particular kinematic bin; the red histogram defines the systematic error and the fit function is $a \sin \Phi/1 + b \cos \Phi$.

V. CONCLUSIONS

Run-group B, which primarily aims to investigate the partonic structure of the neutron and to ultimately achieve, in combination with proton-target experiments, flavor separation of various multi-dimensional structure functions, has run during part of the year 2019, collecting 38.9 PAC days, and with three different electron beam energies. Final and preliminary analyses on the data taken so far show promising results for some the originally proposed measurements as well as for new reaction channels. More statistics is needed in order to be able to sample the multi-dimensional kinematic dependence of the measured observables. For nDVCS, in particular, it is also crucial to be able to collect data with a single value of beam energy. We request the PAC to confirm, for RG-B, the original approved beamtime for the nDVCS experiment (90 days), awarding us therefore 51 more PAC days of running.

REFERENCES

-
- [1] X.-D. Ji, Phys. Rev. Lett. **78**, 610 (1997), arXiv:hep-ph/9603249.
- [2] M. Mazouz *et al.* (Jefferson Lab Hall A), Phys. Rev. Lett. **99**, 242501 (2007), arXiv:0709.0450 [nucl-ex].
- [3] M. Benali *et al.*, Nature Phys. **16**, 191 (2020).
- [4] M. Vanderhaeghen, P. A. Guichon, and M. Guidal, Phys. Rev. D **60**, 094017 (1999), arXiv:hep-ph/9905372.
- [5] A. Bacchetta, M. Diehl, K. Goeke, A. Metz, P. J. Mulders, and M. Schlegel, JHEP **02**, 093 (2007), arXiv:hep-ph/0611265.
- [6] J. Gao, L. Harland-Lang, and J. Rojo, Phys. Rept. **742**, 1 (2018), arXiv:1709.04922 [hep-ph].
- [7] J. J. Ethier and E. R. Nocera, Ann. Rev. Nucl. Part. Sci. **70**, 43 (2020), arXiv:2001.07722 [hep-ph].
- [8] L. Trentadue and G. Veneziano, Phys. Lett. **B323**, 201 (1994).
- [9] M. Anselmino, V. Barone, and A. Kotzinian, Phys. Lett. **B699**, 108 (2011), arXiv:1102.4214 [hep-ph].
- [10] H. Avakian *et al.* (CLAS), Phys. Rev. Lett. **130**, 022501 (2023), arXiv:2208.05086 [hep-ex].
- [11] T. B. Hayward, C. Dilks, A. Vossen, H. Avakian, *et al.* (CLAS Collaboration), Phys. Rev. Lett. **126**, 152501 (2021).
- [12] S. Gliske, A. Bacchetta, and M. Radici, Phys. Rev. D **90**, 114027 (2014), [Erratum: Phys.Rev.D 91, 019902 (2015)], arXiv:1408.5721 [hep-ph].
- [13] A. V. Efremov and P. Schweitzer, JHEP **08**, 006 (2003), arXiv:hep-ph/0212044.
- [14] C.-Y. Seng, Phys. Rev. Lett. **122**, 072001 (2019), arXiv:1809.00307 [hep-ph].
- [15] A. Courtoy, (2014), arXiv:1405.7659 [hep-ph].
- [16] X.-D. Ji, Phys. Rev. Lett. **74**, 1071 (1995), arXiv:hep-ph/9410274.
- [17] M. Burkardt, Phys. Rev. **D88**, 114502 (2013), arXiv:0810.3589 [hep-ph].
- [18] B. Pasquini and S. Rodini, Phys. Lett. B **788**, 414 (2019), arXiv:1806.10932 [hep-ph].
- [19] A. V. Efremov, K. Goeke, and P. Schweitzer, Phys. Rev. **D67**, 114014 (2003), hep-ph/0208124.
- [20] M. Mirazita *et al.* (CLAS), Phys. Rev. Lett. **126**, 062002 (2021), arXiv:2010.09544 [hep-ex].
- [21] A. Bacchetta, G. Bozzi, M. G. Echevarria, C. Pisano, A. Prokudin, and M. Radici, Phys. Lett. B **797**, 134850 (2019), arXiv:1906.07037 [hep-ph].
- [22] S. Gliske, 10.1016/j.physletb.2007.11.096, arXiv:PhD. thesis, <http://www-hermes.desy.de/notes/pub/10-LIB/sgliske.10-003.sidis-vm.pdf> [hep-ph].
- [23] C. Dilks (CLAS), in *28th International Workshop on Deep Inelastic Scattering and Related Subjects* (2021) arXiv:2107.12965 [hep-ex].
- [24] R. L. Jaffe and X.-D. Ji, Nucl. Phys. **B375**, 527 (1992).
- [25] R. Jakob, P. J. Mulders, and J. Rodrigues, Nucl. Phys. **A626**, 937 (1997), hep-ph/9704335.
- [26] C. Cebulla, J. Ossmann, P. Schweitzer, and D. Urbano, Acta Phys. Polon. **B39**, 609 (2008), arXiv:0710.3103 [hep-ph].
- [27] A. Bacchetta and M. Radici, Phys. Rev. **D69**, 074026 (2004), arXiv:hep-ph/0311173.
- [28] A. Ali *et al.* (GlueX Collaboration), Phys. Rev. Lett. **123**, 072001 (2019).
- [29] S. Adhikari *et al.* (GlueX Collaboration), Phys. Rev. C **108**, 025201 (2023).
- [30] B. Duran *et al.* (J/ ψ -007), Nature **615**, 813 (2023), arXiv:2207.05212 [nucl-ex].
- [31] L. Frankfurt and M. Strikman, Phys. Rev. D **66**, 031502 (2002).
- [32] F. Zeng, X.-Y. Wang, L. Zhang, Y. Xie, R. Wang, and X. Chen, The European Physical Journal C **80** (2020), 10.1140/epjc/s10052-020-08584-6.
- [33] D. E. Khazeev, Phys. Rev. D **104**, 054015 (2021).
- [34] Y. Hatta and D.-L. Yang, Phys. Rev. D **98**, 074003 (2018).
- [35] K. A. Mamo and I. Zahed, Phys. Rev. D **106**, 086004 (2022).
- [36] M. Du, V. Baru, F.-K. Guo, C. Hanhart, U.-G. Meissner, A. Nefediev, and I. Strakovsky, The European Physical Journal C **80** (2020), 10.1140/epjc/s10052-020-08620-5.

- [37] D. Winney, C. Fernández-Ramírez, A. Pilloni, A. N. Hiller Blin, M. Albaladejo, L. Bibrzycki, N. Hammoud, J. Liao, V. Mathieu, G. Montaña, R. J. Perry, V. Shastry, W. A. Smith, and A. P. Szczepaniak (Joint Physics Analysis Center), *Phys. Rev. D* **108**, 054018 (2023).
- [38] M. Hattawy *et al.* (CLAS), *Phys. Rev. Lett.* **123**, 032502 (2019), arXiv:1812.07628 [nucl-ex].